Transient optical properties of semiconductors under femtosecond x-ray irradiation

Victor Tkachenko,[1,*] Nikita Medvedev,[1,*] Zheng Li,[1,2] Przemysław Piekarz,[3] and Beata Ziaja[1,3]

[1]*Center for Free-Electron Laser Science CFEL, Deutsches Elektronen-Synchrotron DESY, Notkestrasse 85, 22607 Hamburg, Germany*

[2]*Stanford PULSE Institute, SLAC National Accelerator Laboratory, Menlo Park, California 94025, USA*

[3]*Institute of Nuclear Physics, Polish Academy of Sciences, Radzikowskiego 152, 31-342 Kraków, Poland*

(Received 26 June 2015; revised manuscript received 9 February 2016; published 1 April 2016)

Semiconductors under femtosecond x-ray irradiation are transiently excited to nonequilibrium states. This can lead to observable material modifications. During the excitation and relaxation dynamics, optical properties of the solid are changing, affected by both transient electron excitation as well as the evolution of the atomic structure. In this paper we apply a unified hybrid model to trace these two effects. Transient evolution of the optical properties is calculated within the transferable tight-binding approach. The presented methodology of calculation of the complex dielectric function proves to be capable of describing changes in the optical parameters during the phase transitions, when the solids are driven out of equilibrium by intense laser pulses, in a reasonable agreement with experiments.

DOI: 10.1103/PhysRevB.93.144101

I. INTRODUCTION

Solids under irradiation with femtosecond laser pulses may experience thermal and nonthermal phase transitions [1,2], changing the material structure, or inducing the so-called optical breakdown [3,4]. Optical properties such as reflection, transmission, and absorption are intrinsically related to the electronic state of the target. Experimentally achievable time resolution for measuring the evolution of the optical parameters enables us to follow the transient material excitation and relaxation on a few-femtoseconds time scale [5,6]. Changes of reflectivity, transmission, and absorption coefficients during and after the irradiation can be signatures of electronic excitation or phase transitions within the material [7,8].

Modern free-electron lasers (FELs) producing photons in ultraviolet and x-ray range can generate intense pulses that trigger phase transformations in solids during a single shot [9,10]. Brilliant light sources like FLASH [11], LCLS [12], SACLA [13], and FERMI [14] provide pulses with the duration ranging from a few up to a few tens of femtoseconds. The FEL-triggered electron and lattice dynamics can be studied by the combined FEL pump-optical probe scheme [15–17].

Interaction of short and intense laser pulses with the material leads to a sequence of processes, starting from the absorption of a photon in the x-ray and extreme ultraviolet (XUV) regime [18]. It induces electron transfer from the valence band or deep atomic shells to the conduction band during the exposure to the laser pulse [19]. As a result, a nonequilibrium electron plasma and deep-shell holes can be formed. The core holes decay predominantly via Auger effect for light elements (radiative decay has only negligible contribution) [20]. The excited Auger electrons as well as the photoelectrons then scatter elastically and inelastically. The inelastic scattering produces impact ionization cascades within characteristic time scale of a few femtoseconds, while elastic (phonon) scattering contributes on significantly longer (picosecond) time scales, with only a small fraction of energy transferred in each collision [21]. Electronic excitation also affects the potential energy surface which can lead to a rearrangement of atoms attempting to minimize the potential energy [19]. If this rearrangement is rapid enough and electronic bonds are breaking, a nonthermal phase transition occurs during a few hundred of femtoseconds or even faster, see, e.g., Ref. [22].

For the analysis of experimentally observed changes of the optical properties in laser-irradiated metals, semiconductors, and dielectrics the Drude model is widely applied [23–25]. The model is based on the free-electron gas approximation and calculates the absorption by free carriers. Other details of material structure do not explicitly enter there. Despite this limitation, it is often used as a first-order approximation for modeling and interpretation of experiments [4,25–27].

In this paper we present a developed tight-binding (TB) based model for tracing evolution of optical properties that takes into account both transient changes of the electronic state and of the atomic structure [28]. We also analyze the applicability of the Drude model, comparing it with the calculations using the complex dielectric function (CDF) obtained within the Lindhard random-phase approximation (RPA) in the framework of our TB approach. We show that the evolution of the optical properties under irradiation leading to a phase transition is not described by the Drude model correctly. In contrast, the transferable TB-based approach, albeit being limited to optical wavelengths of the probe pulse, follows the evolution of the optical properties in a very good agreement with the experimental data. This proves its applicability for modeling of excited and relaxing states of matter during phase transitions. The methodology can be easily generalized for a more accurate *ab initio* description of the band structure.

II. MODEL

In this section we describe the methods applied for the description of the optical properties within a laser-irradiated semiconductor. The model for calculation of the complex dielectric function (CDF) and corresponding optical properties is first presented with the focus on its application within the

*Corresponding authors: victor.tkachenko@desy.de and nikita.medvedev@desy.de

tight-binding formalism. XTANT [28], the hybrid model for tracing the evolution of electronic and atomic structure within a laser-excited solid, is then briefly introduced, to explain how the transient properties of the material used for the calculation of the CDF are traced in time.

A. Optical parameters

Optical coefficients of the materials can be expressed in terms of the complex index of refraction $\widetilde{n}$. The reflectivity of the material in the case of the incoming ray incidence with angle θ to the normal in vacuum ($\widetilde{n}_{\rm vac} = 1$) and the propagation with the angle α to the normal in the material, according to Fresnel equations, is defined as

$$R = \left| \frac{\cos\theta - \widetilde{n}\,\cos\alpha}{\cos\theta + \widetilde{n}\,\cos\alpha} \right|^2. \tag{1}$$

From Eq. (1) one can rewrite the expression for reflectivity by using the fact that $\sin\theta = \widetilde{n}\sin\alpha$, as follows from Snell's law, in such a form:

$$R = \left| \frac{\cos\theta - \sqrt{\widetilde{n}^{\,2} - \sin^2\theta}}{\cos\theta + \sqrt{\widetilde{n}^{\,2} - \sin^2\theta}} \right|^2. \tag{2}$$

In Eq. (3) $n(\omega)$ and $k(\omega)$ are the real and imaginary parts of the complex index of refraction, depending on the frequency of the probe pulse ω [29]:

$$\widetilde{n}(\omega) = n(\omega) + ik(\omega). \tag{3}$$

Focusing on the femtosecond laser pulses, and assuming thick material layer, we restrict ourselves to the absorption of the first ray with no interference effects included from multiple reflections on the material boundaries. In this case the corresponding transmission coefficient can be written as [30]

$$T = \left| \frac{4\cos\theta\sqrt{\widetilde{n}^{\,2} - \sin^2\theta}\; e^{-i\,\frac{2\pi d}{\lambda}\sqrt{\widetilde{n}^{\,2}-\sin^2\theta}}}{(\cos\theta + \sqrt{\widetilde{n}^{\,2} - \sin^2\theta})^2} \right|^2, \tag{4}$$

where d is the thickness of the excited material and λ is the wavelength of the incident light. The absorption coefficient can be calculated from the normalization condition

$$A = 1 - T - R. \tag{5}$$

Thus, knowing the complex index of refraction, we can obtain the optical coefficients. For the considered pump-probe scheme with the optical probe pulses, we can apply the dipole approximation $\mathbf{q} = |\mathbf{k} - \mathbf{k}'| \to 0$, where $\mathbf{k}$ and $\mathbf{k}'$ correspond to the crystal momentum in the initial and final state after the optical transition. The complex index of refraction is connected with the complex dielectric function $\epsilon(\omega, \mathbf{q} = \mathbf{0}) \equiv \epsilon(\omega)$:

$$\widetilde{n}(\omega) = \sqrt{\epsilon(\omega)}. \tag{6}$$

In the general relation CDF depends on the optical conductivity of the material $\sigma(\omega)$:

$$\epsilon(\omega) = 1 + i\frac{4\pi\sigma(\omega)}{\omega}. \tag{7}$$

The frequency-dependent CDF can be obtained, e.g., from the density functional theory (DFT) calculations [31]. Among DFT methods, there were estimations for the macroscopic dielectric constant by using, for instance, the full-potential linearized augmented plane wave [32] and the projector-augmented wave methodology [33]. The *ab initio* methods are powerful tools because of their ability to describe equilibrium electronic system of a material with great precision. However, due to their high computational-time demands, it is difficult to apply them to trace evolution of materials in nonequilibrium.

As a consequence, semiempirical methods are frequently applied. They are still able to provide reliable results while describing time-resolved experiments, being not as time consuming and computationally complicated as *ab initio* methods. In this paper we use such a semiempirical tight-binding method based on a set of localized wave functions (see next section).

The complex dielectric function tensor in the random-phase approximation reads as [34]

$$\epsilon^{\alpha\beta}(\omega) = \delta_{\alpha,\beta} + \frac{e^2\hbar^2}{m^2\Omega\, e_0}\sum_{nn'}\frac{F_{nn'}}{E_{nn'}^2}\,\frac{f_{n'} - f_n}{\hbar w - E_{nn'} + i\,\gamma}. \tag{8}$$

Here Ω is the volume of the simulation box, $E_{nn'} = E_{n'} - E_n$ is a transition energy between two eigenstates $|n\rangle$ and $|n'\rangle$, f_n and $f_{n'}$ are the corresponding transient occupation numbers normalized to two (accounting for the spin degeneracy), m is the mass of a free-electron, e is the electron charge, $\hbar$ is the Planck constant, and e_0 is the vacuum permittivity in SI units. Parameter γ is an inverse electron relaxation time. In all following calculations we use $\gamma = 1.5\times10^{13}$ s^{-1}. Particular choice of γ does not affect the results beyond the broadening of peaks in the CDF [35]. $F_{nn'}$ are the oscillator strength corresponding to the energy transition and are defined as

$$F_{nn'} = |\langle n|\hat{p}|n'\rangle|^2, \tag{9}$$

where $\langle n|\hat{p}|n'\rangle$ represents a momentum matrix element between the two eigenstates:

$$\langle n|\hat{p}|n'\rangle = \sum_{\mathbf{R_a}\mathbf{R'_a},\sigma,\sigma'} B_{\sigma\, n}(\mathbf{R_a})P(\mathbf{R_a},\mathbf{R'_a})B_{\sigma'\, n'}(\mathbf{R'_a}). \tag{10}$$

In Eq. (10) $\mathbf{R_a}$ denotes the coordinates of atoms, and σ labels the atomic orbitals. $B_{\sigma\, n}$ and $B_{\sigma'\, n'}$ are the corresponding eigenvectors of the Hamiltonian.

Within the tight-binding model, the momentum matrix elements in Eq. (9) are not directly accessible, because the model does not use an explicit form of electron wave functions. However, by making use of the operator identity $\hat{p} = \frac{m}{i\hbar}[\hat{r}, \hat{H}]$, the momentum matrix elements can be calculated as in [34]:

$$P(\mathbf{R_a},\mathbf{R'_a}) = \frac{m}{i\hbar}[\mathbf{R_a} - \mathbf{R'_a}]H(\mathbf{R_a},\mathbf{R'_a}), \tag{11}$$

where $H(\mathbf{R_a},\mathbf{R'_a})$ is the Hamiltonian matrix. Generally this representation can be applied to any *ab initio* model; in our case, it is used for the tight-binding Hamiltonian, described in Ref. [22] for C, and in Ref. [28] for Si (applied further in the paper).

Since we are interested only in diagonal elements of the complex dielectric function tensor, we calculate three components for the oscillator strength and, correspondingly, for the tensor of the dielectric function. An average value of the CDF is then used:

$$\langle\epsilon\rangle = \tfrac{1}{3}(\epsilon_{xx} + \epsilon_{yy} + \epsilon_{zz}). \tag{12}$$

The final expressions for the real and imaginary part of CDF, entering Eq. (6), are as follows:

$$\mathrm{Re}(\epsilon) = 1 + \frac{e^2\hbar^2}{m^2\Omega\, e_0}\sum_{nn'}\frac{(f_{n'}-f_n)\,F_{nn'}(\hbar\omega - E_{nn'})}{E_{nn'}^2[(\hbar\omega - E_{nn'})^2+\gamma^2]},$$

$$\mathrm{Im}(\epsilon) = -\frac{\gamma\, e^2\hbar^2}{m^2\Omega\, e_0}\sum_{nn'}\frac{(f_{n'}-f_n)\,F_{nn'}}{E_{nn'}^2[(\hbar\omega - E_{nn'})^2+\gamma^2]}. \quad (13)$$

In general, a tight-binding scheme fulfills the Bloch condition for the wave vector k, considering k within the first Brillouin zone. CDF can then be calculated for a number of different k-space points spread over the whole Brillouin zone by averaging contributions from all k points on a mesh in the reciprocal lattice. It is achieved by replacing the Hamiltonian in Eq. (11) by a Fourier transform:

$$H(\mathbf{k}) = \sum_{\mathbf{R}} e^{i\,\mathbf{k}\mathbf{R}} H(\mathbf{R}). \quad (14)$$

The integration in the first Brillouin zone is performed using the Monkhorst-Pack scheme [36].

In comparison, the Drude model, which assumes free-electron approximation, does not include any explicit description of the material band structure or interband transitions [25]. A complex dielectric function in the Drude model is defined as [37]

$$\epsilon(\omega) = \epsilon_0 + \frac{i}{\omega}\frac{{\omega_p}^2\,\tau}{1-i\omega\tau}, \quad (15)$$

where ϵ_0 is the unexcited material dielectric constant, $\omega_p = \sqrt{n_e e^2/m^* e_0}$ is a plasma frequency, with n_e being the free-electron density (of electrons excited to the conduction band) and m^* is the effective electron mass, and τ is a relaxation time. A Drude model with unmodified values of effective electron-hole masses and relaxation time scale is still widely employed for the definition of optical parameters during interpretation of experimental results, e.g., in [24] and [25]. Additionally, we add the terms describing the valence band holes contribution with their effective mass and collision frequency [27]. These parameters are often treated as adjustable parameters. Below we will analyze the applicability of this approach in comparison with the CDF approach in the RPA approximation. Predictions with both models will be compared to experimental results.

B. Modeling material excitation with XTANT

Photons in solids induce a number of processes such as primary photoabsorption, secondary ionizations by high-energy electrons, Auger decays of K-shell holes, and energy exchange with atoms. We use the in-house code XTANT [22,28] to trace the transient electronic as well as atomic dynamics. This hybrid model separates all electrons into high-energy and low-energy fractions. The high-energy electrons are modeled with Monte Carlo method tracing trajectories of individual particles event-by-event, while the low-energy electrons are traced with a temperature model including a Boltzmann collision integral for the electron-ion energy exchange [28]. Thus, the low-energy electrons are characterized by the Fermi distribution function $f(E_n)$ evolving in time according to the changes of the electron chemical potential and temperature. The transient Fermi distributions enter Eqs. (13), together with the transient electron energy levels $E_n = \langle n|\hat{H}|n\rangle$.

The atomic motion is tracked with Ehrenfest molecular dynamics technique (MD). The potential energy surface entering the Newtonian equations of motion for the atoms is obtained from the transferable tight-binding Hamiltonian $\hat{H}$, as described above. We choose an orthogonal sp^3-based transferable tight-binding model, which can accurately reproduce the properties of materials in equilibrium [38,39]. However, due to the limitation of the minimal basis set, this tight-binding model can only satisfactorily describe band structure of the valence band and of the bottom of the conduction band. This affects the accuracy of modeling CDF at higher photon energies, when a certain number of electrons is excited to high-lying states in the conduction band [40]. This limitation will be analyzed in the next section.

III. RESULTS

A. Validation of the model

We start by calculating the spectrum of the optical parameters [$n(\omega)$ and $k(\omega)$ indices, Eq. (3)] for unirradiated materials: diamond and silicon. An example of the $n(\omega)$ and $k(\omega)$ calculated with Eqs. (3), (13), and (14) in diamond is shown in Fig. 1. Experimental points taken from Ref. [41] and theoretical results (obtained with DFT calculations) extracted from [42] are shown for comparison. We analyzed the dependence of the calculated spectra on the number of $\mathbf{k}$ points: for the Γ-point calculation ($\mathbf{k} = 0$), the $n(\omega)$ and

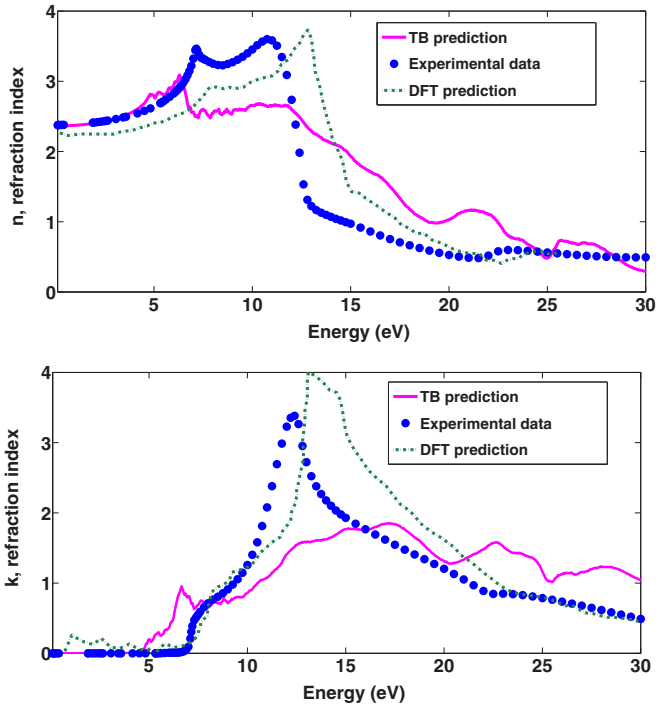

FIG. 1. Optical refractive indices n and k of the equilibrium diamond. The dots are experimental data [41], the dot-dashed line is calculated with DFT method [42], and the solid line is a TB curve obtained with 1728 k points in the simulation.

$k(\omega)$ coefficients follow the experimental values only at the low energies, below ∼7 eV, after which they exhibit strong oscillations (not shown). As expected, the amplitude of these oscillations decreases with the increase of the number of points in the grid in **k** space. It converges for the number of points greater than ∼200.

As shown in Fig. 1 the components of complex refractive index $n(\omega)$ and $k(\omega)$ are in qualitative agreement with the experiment, although the broad peak at ∼12 eV is missing due to the incapability of the TB model to accurately describe high-lying states in the conduction band. More precise calculations of the dielectric function in equilibrium can be done in a framework of an *ab initio* method based on density functional theory or by constructing a new set of tight-binding parameters [40,43,44]. However, the main point of the present work is to study material evolution under a laser pulse irradiation, which requires *transferable* tight binding coefficients.

Moreover, we are focusing here on the optical probe (photon energies below ∼2 eV), for which the presented TB method shows a very good agreement with the experimental $n(\omega)$ and $k(\omega)$ points. Interestingly, for the low energies even the calculations for only the Γ-point produce results accurate enough. As the numerical investigation of transient processes in irradiated diamond is computationally demanding, the Γ-point approximation can be used for reducing the computational costs.

The same approach has been applied to silicon. The results are shown in Fig. 2. They show convergence for ∼200 **k** points, however with poorer agreement with the data. Here the sharp peaks observed in experimental data are missing. Moreover, the agreement at low energies is limited to energies below

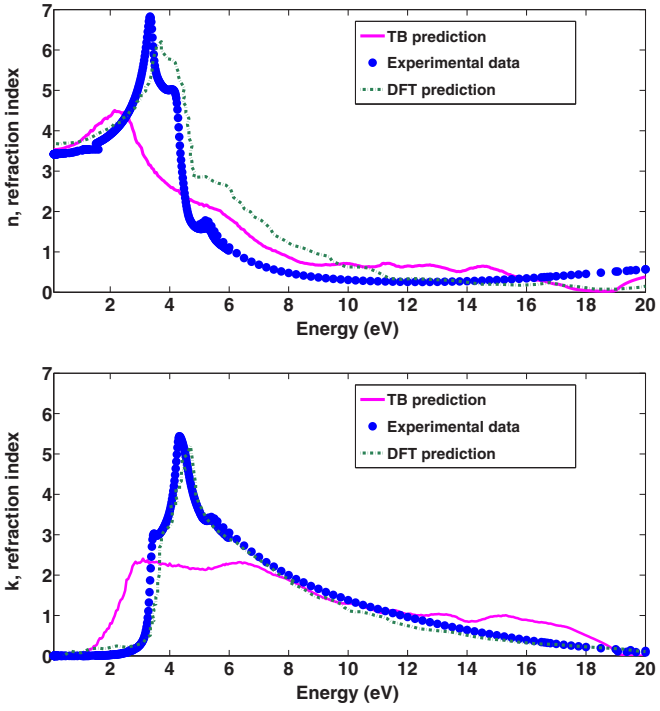

FIG. 2. Optical refractive indices n and k of the equilibrium silicon. The dots are experimental data [41], the dot-dashed line is calculated with DFT method [42], and the solid line is a TB curve obtained for 216 k points used in the simulation.

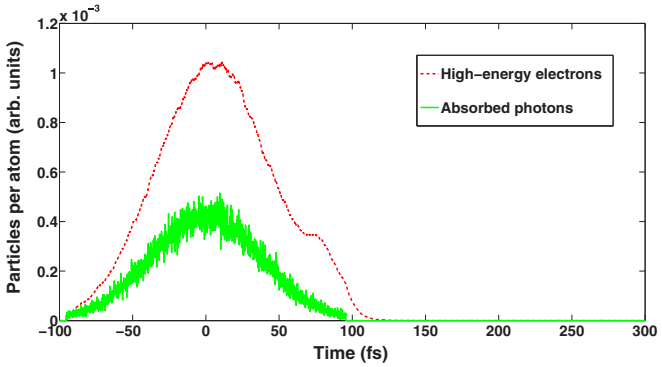

FIG. 3. The number of high-energy electrons (with energies above 10 eV) and absorbed photons in excited diamond (in arbitrary units). FEL photon energy = 50 eV, pulse duration = 90 fs, absorbed dose = 1.0 eV/atom.

∼2 eV only. This is, however, still sufficient for the description of pump-probe experiments with optical probe pulses.

Apart from increasing the number of **k** points, we analyzed another possibility of improving the simulation accuracy by increasing of the number of the atoms (N) in the simulation box. This attempt proved to be even more computational-time consuming due to the high N scaling in the diagonalizing subroutine, and to the worse convergence properties. Even for 1000 atoms, the results did not converge better than for 8 **k** points and 64 atoms.

After the detailed discussion of the limitations within our model, we can proceed with the investigation of the transient optical parameters in irradiated materials.

B. Evolution of optical parameters within irradiated material

We begin with a study of the evolution of the optical parameters in irradiated diamond. In our simulation, diamond is irradiated with the 90-fs-long pulse of the Gaussian temporal profile, the photon energy is 50 eV, and the fluence is varied around the damage threshold (below and above the graphitization threshold which is ∼0.7 eV/atom [22]).

First of all, to benchmark the calculations, we make an illustrative comparison of our results to the time-resolved experimental data—currently available from the optical regime only. In the experiment performed by Reitze *et al.* [26], an optical laser pump pulse was used. However, our model considers only single photon absorption, hence it is limited to photon energies above approximately 30 eV. Nonetheless, we can compare our results with those ones, because after the irradiation with 50 eV photons, electron cascading is extremely fast [45]. High-energy electrons are relaxed to low energy states within a few femtoseconds (see Fig. 3), after which the material conditions become close to the case of optical pulse irradiation. Thermalization of electrons in solids on a time scale of a few femtoseconds has been observed in various experiments with optical pumping of solids as well [46,47].

In this experiment [26] the absorbed dose was 9 times the damage threshold fluence, i.e., approximately 6.3 eV/atom. According to the experimental parameters, the optical probe pulse used in our simulations is 620 nm (∼2 eV). The probe pulse in the experiment was incident at a large enough

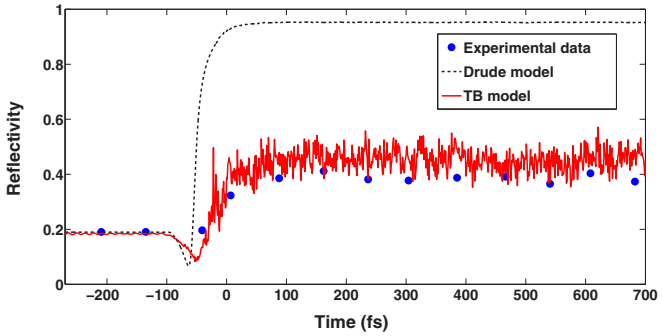

FIG. 4. Reflectivity coefficient of diamond irradiated with the absorbed dose of 6.3 eV/atom. Probe pulse of 620 nm and angle of incidence of 20° is used. The dots are experimental data [26], the solid line is the TB calculations, and the dashed line is the Drude model.

angle (20°), so the front surface reflection has been spatially separated from the back surface reflection [26]. As in the model we also excluded interference effects from the calculations [see Eqs. (2) and (4)], the results predicted by the model can be directly compared to the experimental data.

The initial electron and atom temperatures are equal to the room temperature (300 K). A constant volume simulation scheme is used, assuming that the considered time scales are too short for any macroscopic relaxation processes that could reduce the density of the material. In what follows the calculations always include 216 atoms in the simulation box. We choose a sample thickness d equal to the attenuation length of the photons of 50 eV energy for the selected material [48]. In case of XUV pump pulse, $d \sim 100$ nm.

One can see in Fig. 4 that before the laser pulse arrives, our calculations reproduce the optical properties accurately, in accordance with the results presented in the previous section. A small dip in the simulation around the pulse maximum could be a result of different transient nonequilibrium electron distributions in the model and in the experiment, as was mentioned in this section above. Calculations with the Drude model, Eq. (15), are also shown for comparison. Here the free-model parameters were fitted to reproduce the correct initial values at equilibrium.

Figure 4 demonstrates that the changes of reflectivity are reproduced very well within our TB model for the complex dielectric function, even during the extremely fast nonthermal phase transition to graphite, which occurs within ~50–70 fs [22]. The final excited graphite state is also close to the experimental points.

In contrast, the Drude model follows the data only at low irradiation dose (at the beginning of the laser pulse). Our study demonstrates that the results of the Drude model with a fixed scattering time agree well with the detailed simulation in the framework of TB-RPA calculations in the regime when there is no significant atomic heating and significant changes in the electronic band structure (such as band gap closure). In the case of diamond, it appears to be for the absorbed doses below 0.3 eV/atom. As soon as the excited electron density overcomes the so-called optical breakdown threshold, the Drude model predicts nearly full reflection, in a striking disagreement with the experiment. This is due to

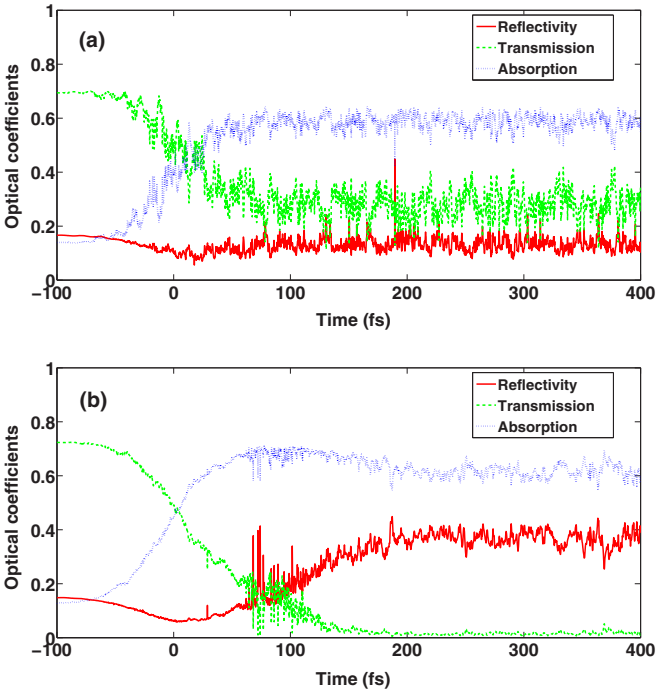

FIG. 5. Modeled optical coefficients of diamond irradiated below the damage threshold (a) with the dose = 0.6 eV/atom, and above the threshold (b) with the dose = 1.0 eV/atom. The solid lines represent the reflectivity coefficient, the dashed lines are transmission coefficients, and the dotted lines are absorption coefficients.

the fact that the Drude model's applicability is limited to low radiation doses, below the damage and "optical breakdown" thresholds [25]. The Drude model does not account for atomic rearrangement during strong excitation and phase transition, the corresponding changes in electronic band structure, and the interband transitions.

In the present simulation fixed values are used for effective conduction-band electron and valence-band hole masses, and for the electron scattering time (assumed here to be 1 fs). By allowing the scattering time to change, one could better reproduce the experimental data [49]. However, the evolution of the material structure cannot be self-consistently included in the Drude model.

As we showed that the developed TB model reproduces dynamical changes of the optical properties in highly excited diamond, we can now study in more detail the near-threshold behavior. When the absorbed fluences are close to the damage threshold, we can see how the phase transition affects the transient optical properties of diamond.

Figure 5 presents results on diamond irradiated with 0.6 and 1 eV per atom of the absorbed dose, 90 fs FWHM pump pulse. The probe pulse is 600 nm wavelength (photon energy 2.07 eV) under the perpendicular incidence to the sample; the FEL pulse is of 50 eV photon energy, 90 fs duration.

For the below-threshold dose (0.6 eV/atom), Fig. 5(a) shows that the transmission decreases during the irradiation from ~0.7 to ~0.3, never vanishing completely. The absorption also changes significantly, while the reflectivity is only slightly affected. These effects can be attributed to transient electron excitation.

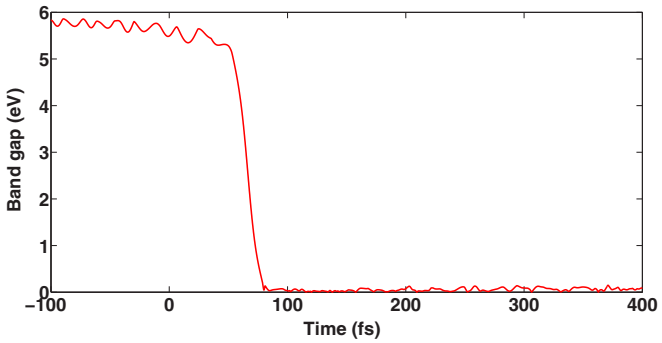

FIG. 6. Band gap of diamond after irradiation with laser pulse at the absorbed dose of 1.0 eV/atom, $\hbar w = 50$ eV, and pulse duration $\tau = 90$ fs.

On longer time scales we expect the optical coefficients to return to their original values (as they were in the undamaged material). In our model with periodic boundary conditions, there is no energy transport included, which precludes us from the direct observation of this relaxation stage.

Figure 5(b) shows that above the graphitization threshold the transmission coefficient of diamond drops to zero from the initial value of approximately 0.7 at about 100 fs. At the same time the reflectivity coefficient rises. It takes some time for atoms to relax nonthermally to the new phase of graphite [19]. When it occurs, the transmission drops to zero, corresponding to a nontransparent graphite state.

The fact that the drop of transmission indicates a phase transition can be proved by examining other signatures of the graphitization. As it was studied in detail in Ref. [22], at the beginning of of the graphitization process the diamond bonds start breaking. This leads to the band gap collapse (see Fig. 6). Later, the structure becomes graphitelike with parallel atomic planes (see Fig. 7), and transmission finally drops to zero [see Fig. 5(b)].

As band gap shrinkage is a signature and a trigger of nonthermal phase transition [19], by following the band gap dynamics we may reconstruct the mechanism of the phase transition. Band gap width is connected with frequency dependent optical conductivity $\sigma(\omega)$. It has an onset frequency that characterizes the interband electron transition. Furthermore, the time-resolved optical conductivity can be measured in experiments [50–52] and hence this can be used as an insightful tool for the investigation of phase transitions.

Defining CDF of a solid as a function of frequency and time, we can calculate transient optical conductivity spectrum by using Eq. (7) (see Fig. 8). In a nonexcited equilibrium

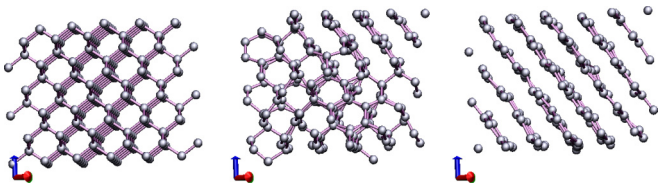

FIG. 7. Snapshots of carbon atomic positions in the supercell at different moments of time: −100 fs (left), 150 fs (center), 400 fs (right). Absorbed dose is 1.0 eV/atom, $\hbar w = 50$ eV, pulse duration $\tau = 90$ fs.

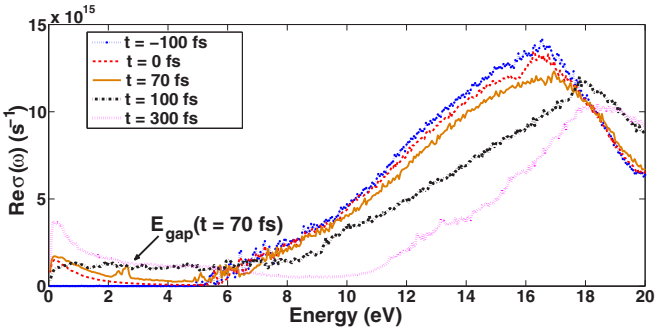

FIG. 8. Frequency-dependent optical conductivity in diamond (graphite) at various time instants during graphitization: $t = -100$, 0, 70, 100, 300 fs.

diamond, optical conductivity has nonzero values, starting from the edge of a band gap as expected from the theory (Fig. 8, $t = -100$ fs). At $t = 70$ fs, during the graphitization, the first resonant peak (marked on Fig. 8) shows up. When the sample is fully graphitized (Fig. 8, 300 fs) there is no trace of a band gap in semimetalic graphite, as expected.

Now let us analyze the second material under investigation: silicon. Its threshold dose for phase transition into low-density-liquid phase is about 0.6–0.65 eV/atom; the nonthermal melting into a high-density liquid phase occurs for doses above 0.9 eV on the time scale of about 300 fs [28]. In the experiment performed by Sokolowski-Tinten *et al.* [27] on irradiation of silicon, an optical pulse with 625 nm wavelength was used. In our model, again, we apply the photon energy of 50 eV for a pump pulse, while using 625 nm wavelength for the probe. The absorbed dose is 1 eV/atom which can be compared with the data on 1.8 times the threshold dose for silicon shown in Ref. [27]. The pump pulse duration is 100 fs.

Figure 9 shows a good agreement of our model with experimental results, despite the less accurate reproduction of the unirradiated optical parameters. Similarly to the case of diamond, at the instance of a phase transition, the transmission

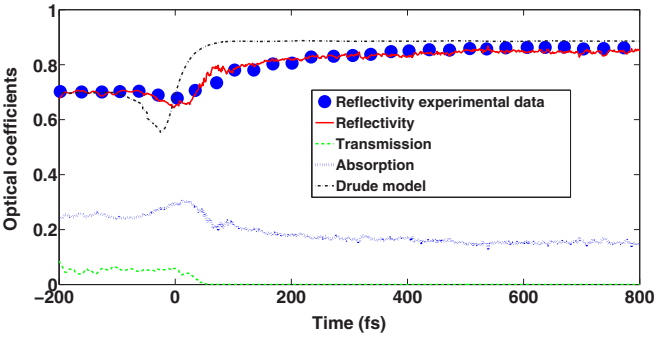

FIG. 9. Modeled optical coefficients of nonequilibrium silicon irradiated above the damage threshold, at the absorbed dose = 1.0 eV/atom, $\hbar w = 50$ eV, pulse duration $\tau = 100$ fs. Angle of the pulse incidence is 70.5°. The dots represent experimental data for reflectivity coefficient, the solid line represents the calculated reflectivity coefficient, the dashed line is the calculated transmission coefficient, the dotted line is the calculated absorption coefficient obtained within TB model, and the dot-dashed line is the reflectivity coefficient obtained within the Drude model.

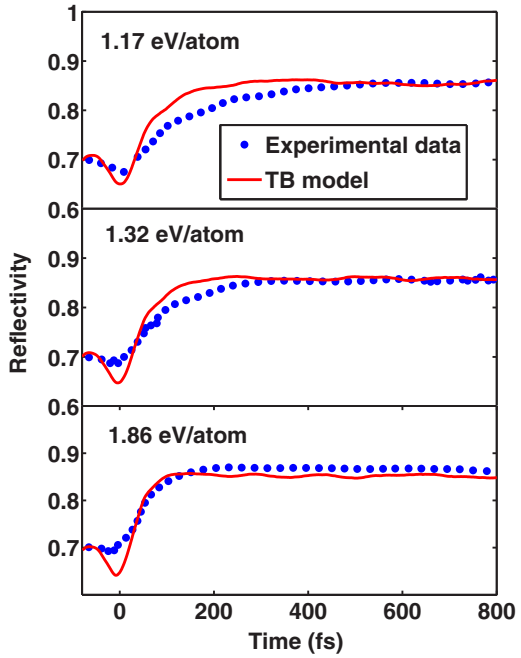

FIG. 10. Reflectivity of silicon measured in the experiment [27] in comparison with TB model predictions for various absorbed doses.

coefficient drops to zero, and simultaneously reflectivity and absorption coefficients temporarily rise up (see Fig. 9). Here the phase transition is the nonthermal melting into high-density liquid state (see details in Ref. [28]). It also proceeds with the band gap collapse and further atomic rearrangement leading to amorphization. This affects the reflectivity on the transition-specific time scales, thus, the experimental observation of the fast rise of reflectivity can indeed be interpreted as a sign of nonthermal phase transition [27]. Comparison for reflectivity at other above-threshold fluences used in the experiment [27] is shown in Fig. 10. The comparison looks satisfactory for the values before and after the pulse, while some differences during the pulse can be noticed. Similarly to the case of diamond discussed above, during and slightly after the pulse, the nonequilibrium electronic state in the model (XUV excitation) can differ from the experimental one (optical irradiation), thus some differences before the electron thermalization should be expected. The minor dip and faster raise of the calculated reflectivity seem to indicate this differences.

The current model is limited to high fluences (above the nonthermal melting threshold). Although lower fluences producing thermal heating and melting in silicon can, in principle, be modeled with our approach, other limitations of the current model restrict such application. For example, since the thermal melting takes significantly longer times (picoseconds), at such time scales particle and heat diffusion can no longer be neglected. They affect the optical properties observed experimentally. Accounting for such effects is beyond of scope of the present paper; we limit ourselves to a few data sets with fluences above the nonthermal melting, which is then the dominant process, sufficiently fast to apply our current approach.

The fact that the nonthermal phase transition could be reproduced with a satisfactory accuracy (Figs. 4 and 9) shows that the developed approach of CDF calculations within the TB model is capable of describing excited and nonequilibrium transient states of irradiated materials. This model can then be used for interpretations of future and on-going FEL pump-optical probe experiments on semiconductors.

IV. CONCLUSIONS

In this paper we analyzed transient optical properties of diamond and silicon under femtosecond laser pulse irradiation. We applied a transferable tight-binding approach to calculate the complex dielectric function. The results showed reasonable agreement with the available experimental data for both materials. The discrepancy between predictions and the data during the optical pulse and several femtoseconds afterwards was due to the effects specific to optical irradiation which are not included into our model. Nonthermal phase transitions manifested themselves as a drop of the optical transmission and the raise of reflectivity, which can be monitored in pump-probe experiments with femtosecond resolution. Clear signature of the below-damage and above-damage irradiation was found in the predicted optical coefficients. It was also demonstrated that the Drude model worked only in the low-excitation limit, below the optical breakdown. For higher excitation, the model drastically overestimated the experimental reflectivity in diamond, while the tight-binding-based calculations still agreed well with the experiments.

ACKNOWLEDGMENTS

The authors thank Daniele Nicoletti, Robin Santra, Franz Tavella, Sven Toleikis and Oriol Vendrell for valuable discussions. Z. L. thanks the Volkswagen Foundation for support through a Paul-Ewald postdoctoral fellowship.

[1] A. Rousse, C. Rischel, S. Fourmaux, I. Uschmann, S. Sebban, G. Grillon, Ph. Balcou, E. Frster, J. P. Geindre, P. Audebert, J. C. Gauthier, and D. Hulin, Nature (London) **410**, 65 (2001).
[2] S. K. Sundaram and E. Mazur, Nat. Matter. **1**, 217 (2002).
[3] M. Lenzner, J. Krger, S. Sartania, Z. Cheng, Ch. Spielmann, G. Mourou, W. Kautek, and F. Krausz, Phys. Rev. Lett. **80**, 4076 (1998).
[4] N. Medvedev and B. Rethfeld, J. Appl. Phys. **108**, 103112 (2010).
[5] N. Del Fatti, C. Voisin, M. Achermann, S. Tzortzakis, D. Christofilos, and F. Valle, Phys. Rev. B **61**, 16956 (2000).
[6] C. K. Sun, F. Valle, L. Acioli, E. P. Ippen, and J. G. Fujimoto, Phys. Rev. B **48**, 12365 (1993).

[7] H. O. Jeschke, M. E. Garcia, and K. H. Bennemann, Phys. Rev. B **60**, R3701 (1999).

[8] O. Krupin, M. Trigo, W. F. Schlotter, M. Beye, F. Sorgenfrei, J. J. Turner, D. A. Reis, N. Gerken, S. Lee, W. S. Lee, G. Hays, Y. Acremann, B. Abbey, R. Coffee, M. Messerschmidt, S. P. Hau-Riege, G. Lapertot, J. Lning, P. Heimann, R. Soufli, M. Fernndez-Perea, M. Rowen, M. Holmes, S. L. Molodtsov, A. Fhlisch, and W. Wurth, Opt. Express **20**, 11396 (2012).

[9] J. B. Pelka, R. Sobierajski, D. Klinger, W. Paszkowicz, J. Krzywinski, M. Jurek, D. Zymierska, A. Wawro, A. Petroutchik, L. Juha, V. Hajkova, J. Cihelka, J. Chalupsky, T. Burian, L. Vysin, S. Toleikis, K. Sokolowski-Tinten, N. Stojanovic, U. Zastrau, R. London, S. Hau-Riege, C. Riekel, R. Davies, M. Burghammer, E. Dynowska, W. Szuszkiewicz, W. Caliebe, and R. Nietubyc, Radiat. Phys. Chem. **78**, S46 (2009).

[10] S. Hellmann, C. Sohrt, M. Beye, T. Rohwer, F. Sorgenfrei, M. Marczynski-Bhlow, M. Kallne, H. Redlin, F. Hennies, M. Bauer, A. Fhlisch, L. Kipp, W. Wurth, and K. Rossnagel, New J. Phys. **14**, 013062 (2012).

[11] W. Ackermann, G. Asova, V. Ayvazyan, A. Azima, N. Baboi, J. Bhr, V. Balandin, B. Beutner, A. Brandt, A. Bolzmann, R. Brinkmann, O. I. Brovko, M. Castellano, P. Castro, L. Catani, E. Chiadroni, S. Choroba, A. Cianchi, J. T. Costello, D. Cubaynes, J. Dardis, W. Decking, H. Delsim-Hashemi, A. Delserieys, G. Di Pirro, M. Dohlus, S. Dsterer, A. Eckhardt, H. T. Edwards, B. Faatz, J. Feldhaus, K. Flttmann, J. Frisch, L. Frhlich, T. Garvey, U. Gensch, Ch. Gerth, M. Grler, N. Golubeva, H.-J. Grabosch, M. Grecki, O. Grimm, K. Hacker, U. Hahn, J. H. Han, K. Honkavaara, T. Hott, M. Hning, Y. Ivanisenko, E. Jaeschke, W. Jalmuzna, T. Jezynski, R. Kammering, V. Katalev, K. Kavanagh, E. T. Kennedy, S. Khodyachykh, K. Klose, V. Kocharyan, M. Krfer, M. Kollewe, W. Koprek, S. Korepanov, D. Kostin, M. Krassilnikov, G. Kube, M. Kuhlmann, C. L. S. Lewis, L. Lilje, T. Limberg, D. Lipka, F. Lhl, H. Luna, M. Luong, M. Martins, M. Meyer, P. Michelato, V. Miltchev, W. D. Mller, L. Monaco, W. F. O. Mller, O. Napieralski, O. Napoly, P. Nicolosi, D. Nlle, T. Nuez, A. Oppelt, C. Pagani, R. Paparella, N. Pchalek, J. Pedregosa-Gutierrez, B. Petersen, B. Petrosyan, G. Petrosyan, L. Petrosyan, J. Pflger, E. Plnjes, L. Poletto, K. Pozniak, E. Prat, D. Proch, P. Pucyk, P. Radcliffe, H. Redlin, K. Rehlich, M. Richter, M. Roehrs, J. Roensch, R. Romaniuk, M. Ross, J. Rossbach, V. Rybnikov, M. Sachwitz, E. L. Saldin, W. Sandner, H. Schlarb, B. Schmidt, M. Schmitz, P. Schmser, J. R. Schneider, E. A. Schneidmiller, S. Schnepp, S. Schreiber, M. Seidel, D. Sertore, A. V. Shabunov, C. Simon, S. Simrock, E. Sombrowski, A. A. Sorokin, P. Spanknebel, R. Spesyvtsev, L. Staykov, B. Steffen, F. Stephan, F. Stulle, H. Thom, K. Tiedtke, M. Tischer, S. Toleikis, R. Treusch, D. Trines, I. Tsakov, E. Vogel, T. Weiland, H. Weise, M. Wellhfer, M. Wendt, I. Will, A. Winter, K. Wittenburg, W. Wurth, P. Yeates, M. V. Yurkov, I. Zagorodnov, and K. Zapfe, Nat. Photon. **1**, 336 (2007).

[12] P. Emma, R. Akre, J. Arthur, R. Bionta, C. Bostedt, J. Bozek, A. Brachmann, P. Bucksbaum, R. Coffee, F.-J. Decker, Y. Ding, D. Dowell, S. Edstrom, A. Fisher, J. Frisch, S. Gilevich, J. Hastings, G. Hays, Ph. Hering, Z. Huang, R. Iverson, H. Loos, M. Messerschmidt, A. Miahnahri, S. Moeller, H.-D. Nuhn, G. Pile, D. Ratner, J. Rzepiela, D. Schultz, T. Smith, P. Stefan, H. Tompkins, J. Turner, J. Welch, W. White, J. Wu1, G. Yocky, and J. Galayda, Nat. Photon. **4**, 641 (2010).

[13] D. Pile, Nat. Photon. **5**, 456 (2011).

[14] E. Allaria, R. Appio, L. Badano, W. A. Barletta, S. Bassanese, S. G. Biedron, A. Borga, E. Busetto, D. Castronovo, P. Cinquegrana, S. Cleva, D. Cocco, M. Cornacchia, P. Craievich, I. Cudin, G. D'Auria, M. Dal Forno, M. B. Danailov, R. De Monte, G. De Ninno, P. Delgiusto, A. Demidovich, S. Di Mitri, B. Diviacco, A. Fabris, R. Fabris, W. Fawley, M. Ferianis, E. Ferrari, S. Ferry, L. Froehlich, P. Furlan, G. Gaio, F. Gelmetti, L. Giannessi, M. Giannini, R. Gobessi, R. Ivanov, E. Karantzoulis, M. Lonza, A. Lutman, B. Mahieu, M. Milloch, S. V. Milton, M. Musardo, I. Nikolov, S. Noe, F. Parmigiani, G. Penco, M. Petronio, L. Pivetta, M. Predonzani, F. Rossi, L. Rumiz, A. Salom, C. Scafuri, C. Serpico, P. Sigalotti, S. Spampinati, C. Spezzani, M. Svandrlik, C. Svetina, S. Tazzari, M. Trovo, R. Umer, A. Vascotto, M. Veronese, R. Visintini, M. Zaccaria, D. Zangrando, and Zangrando, Nat. Photon. **6**, 699 (2012).

[15] T. Maltezopoulos, S. Cunovic, M. Wieland, M. Beye, A. Azima, H. Redlin, M. Krikunova, R. Kalms, U. Frhling, F. Budzyn, W. Wurth, A. Fhlisch, and M. Drescher, New J. Phys. **10**, 033026 (2008).

[16] M. Harmand, R. Coffee, M. R. Bionta, M. Chollet, D. French, D. Zhu, D. M. Fritz, H. T. Lemke, N. Medvedev, B. Ziaja, S. Toleikis, and M. Cammarata, Nat. Photon. **7**, 215 (2013).

[17] R. Riedel, A. Al-Shemmary, M. Gensch, T. Golz, M. Harmand, N. Medvedev, M. J. Prandolini, K. Sokolowski-Tinten, S. Toleikis, U. Wegner, B. Ziaja, N. Stojanovic, and F. Tavella, Nat. Commun. **4**, 1731 (2013).

[18] N. Medvedev and B. Rethfeld, New J. Phys. **12**, 073037 (2010).

[19] N. Medvedev, V. Tkachenko, and B. Ziaja, Contrib. Plasma Phys. **55**, 12 (2015).

[20] O. Keski-Rahkonen and M. O. Krause, Atom. Data Nucl. Data Tabl. **14**, 139 (1974).

[21] P. Lorazo, L. Lewis, and M. Meunier, Phys. Rev. B **73**, 134108 (2006).

[22] N. Medvedev, H. O. Jeschke, and B. Ziaja, New J. Phys. **15**, 015016 (2013).

[23] D. Puerto, J. Siegel, W. Gawelda, M. Galvan-Sosa, L. Ehrentraut, J. Bonse, and J. Solis, J. Opt. Soc. Am. B **27**, 1065 (2010).

[24] D. Fisher, M. Fraenkel, Z. Henis, E. Moshe, and S. Eliezer, Phys. Rev. E **65**, 016409 (2002).

[25] B. Rethfeld, O. Brenk, N. Medvedev, H. Krutsch, and D. H. H. Hoffmann, Appl. Phys. A **101**, 19 (2010).

[26] D. H. Reitze, H. Ahn, and M. C. Downer, Phys. Rev. B **45**, 2677 (1992).

[27] K. Sokolowski-Tinten, J. Bialkowski, D. von der Linde, Phys. Rev. B **51**, 14186 (1995).

[28] N. Medvedev, Z. Li, and B. Ziaja, Phys. Rev. B **91**, 054113 (2015).

[29] J. P. Mathieu, *Optics* (Pergamon Press, Oxford, 1975).

[30] P. Yeh, *Optical Waves in Layered Media* (Wiley, New York).

[31] S. Baroni and R. Resta, Phys. Rev. B **33**, 7017 (1986).

[32] P. Puschnig and C. Ambrosch-Draxl, Phys. Rev. B **66**, 165105 (2002).

[33] M. Gajdos, K. Hummer, and G. Kresse, Phys. Rev. B **73**, 045112 (2006).

[34] F. Trani, G. Cantele, D. Ninno, and G. Iadonisi, Phys. Rev. B **72**, 075423 (2005).

[35] C. F. Klingshirn, *Semiconductor Optics* (Springer, Berlin, 1997).

[36] H. J. Monkhorst and J. D. Pack, Phys. Rev. B **13**, 5188 (1976).
[37] H. P. Gail and E. Sedlmayr, *Physics and Chemistry of Circumstellar Dust Shells* (Cambridge University Press, Cambridge, 2014).
[38] C. H. Xu, C. Z. Wang, C. T. Chan, and K. M. Ho, J. Phys.: Condens. Matter **4**, 6047 (1992).
[39] I. Kwon, R. Biswas, C. Z. Wang, K. M. Ho, and C. M. Soukoulis, Phys. Rev. B **49**, 7242 (1994).
[40] J. L. Mercer, Phys. Rev. B **54**, 4650 (1996).
[41] E. D. Palik, *Handbook of Optical Constants of Solids* (Academic Press, New York, 1985).
[42] X. Liu, L. Li, and F. Lu, arXiv:1301.1745.
[43] Y. M. Niquet, C. Delerue, G. Allan, and M. Lannoo, Phys. Rev. B **62**, 5109 (2000).
[44] C. Tserbak, H. M. Polatoglou, and G. Theodorou, Phys. Rev. B **47**, 7104 (1993).
[45] N. Medvedev, Appl. Phys. B **118**, 417 (2015).
[46] T. Hertel, E. Knoesel, M. Wolf, and G. Ertl, Phys. Rev. Lett. **76**, 535 (1996).
[47] A. Giri and P. E. Hopkins, J. Appl. Phys. **118**, 215101 (2015).
[48] B. L. Henke, E. M. Gullikson, and J. C. Davis, At. Data Nucl. Data Tables **54**, 181 (1993).
[49] A. Rämer, O. Osmani, and B. Rethfeld, J. Appl. Phys. **116**, 053508 (2014).
[50] G. A. Thomas, M. Capizzi, F. DeRosa, R. N. Bhatt, and T. M. Rice, Phys. Rev. B **23**, 5472 (1981).
[51] R. Huber, F. Tauser, A. Brodschelm, M. Bichler, G. Abstreiter, and A. Leitenstorfer, Nature (London) **414**, 286 (2001).
[52] R. Singla, G. Cotugno, S. Kaiser, M. Frst, M. Mitrano, H. Y. Liu, A. Cartella, C. Manzoni, H. Okamoto, T. Hasegawa, S. R. Clark, D. Jaksch, and A. Cavalleri, Phys. Rev. Lett. **115**, 187401 (2015).